nature chemistry

ARTICLES

PUBLISHED ONLINE: 16 FEBRUARY 2015 | DOI: 10.1038/NCHEM.2180

Stereoelectronic switching in single-molecule junctions

Timothy A. Su[1], Haixing Li[2], Michael L. Steigerwald[1]*, Latha Venkataraman[2]* and Colin Nuckolls[1]*

A new intersection between reaction chemistry and electronic circuitry is emerging from the ultraminiaturization of electronic devices. Over decades chemists have developed a nuanced understanding of stereoelectronics to establish how the electronic properties of molecules relate to their conformation; the recent advent of single-molecule break-junction techniques provides the means to alter this conformation with a level of control previously unimagined. Here we unite these ideas by demonstrating the first single-molecule switch that operates through a stereoelectronic effect. We demonstrate this behaviour in permethyloligosilanes with methylthiomethyl electrode linkers. The strong σ conjugation in the oligosilane backbone couples the stereoelectronic properties of the sulfur–methylene σ bonds that terminate the molecule. Theoretical calculations support the existence of three distinct dihedral conformations that differ drastically in their electronic character. We can shift between these three species by simply lengthening or compressing the molecular junction, and, in doing so, we can switch conductance digitally between two states.

The development of single-molecule conductance switches is crucial to the realization of nanoscale electronic devices in which molecules will serve as components in electrical circuitry[1,2]. Controlling the electronic properties of single molecules in the context of electronic devices is a relatively new field of interest; however, chemists have studied the electronic properties of molecules in the context of chemical reactivity over many decades. Incorporating the paradigms of reaction chemistry into the design of molecular electronic components can provide a tremendous impetus to advance the field of molecular electronics. For example, chemical principles such as photocyclization[3], tautomerization[4] and cross-conjugation[5] have inspired the genesis of many new types of molecular electronic components[6–8].

Here we introduce the first example of a molecular electronic switch that operates through a stereoelectronic effect. Stereoelectronic effects are fundamental to reaction chemistry because they determine how the properties and reactivities of molecules depend on the relative spatial orientations of their electron orbitals[9]. The vast stereoelectronics knowledge base can therefore serve as a tremendous resource in controlling electronics at the single-molecule level by directing molecular conformation. Although conformational effects have been reported in other single-molecule devices, none of these reported components have demonstrated digital switching between conductance states by controlling bond rotation, as is shown here[10–15].

We utilize the sub-ångström level of control in a scanning tunnelling microscope-based break-junction (STM-BJ) technique to manipulate specific dihedral angles in permethyloligosilanes with aurophilic methylthiomethyl electrode contacts (Fig. 1). We can increase the conductance by elongating the molecular junction and decrease the conductance by compressing the electrodes; each terminal (C–S–C–Si) dihedral angle that couples the electrode-linker orbital into the σ framework acts as a gate to control conductance. We find an analogy in the computational studies of Franco *et al.*, who predicted the same principle in a cyclophane in which junction elongation opens a more conductive channel for transport[16]. The switching that we see is binary in the sense that there are only two discrete conductances. We see no evidence of intermediate conductance values, and therefore the switching is faster than the microsecond time resolution of the STM.

Results and discussion

Synthetic design. Figure 2 shows the iterative synthesis we devised for the $[SiMe_2]_n$ oligosilanes ($n = 1$–10) terminated by methylthiomethyl linkers (**Si1**–**Si10**). We grew α,ω-diphenyloligosilane **2** outwards, two silicon subunits at a time, by treating α,ω-dichlorooligosilane **3** with two equivalents of dimethylphenylsilyl magnesium **1**[17]. Protodesilylation of α,ω-diphenyloligosilane **2** under acidic conditions furnished the chain-extended α,ω-dichlorooligosilane **3**[18]. The odd and even series were built

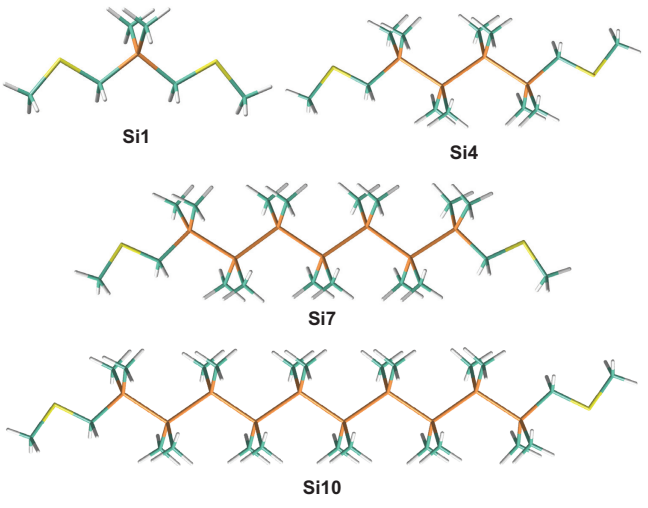

Figure 1 | Structures of oligosilanes Si1, Si4, Si7 and Si10 calculated at the B3LYP/6-31G level.** The backbone (Si–Si–Si–Si) dihedral angles are held to 180° to emphasize the length difference across the oligosilane series. Si, orange; C, teal; S, yellow; H, grey.

[1]Department of Chemistry, Columbia University, New York 10027, USA. [2]Department of Applied Physics, Columbia University, New York 10027, USA. *e-mail: cn37@columbia.edu; mls2064@columbia.edu; lv2117@columbia.edu

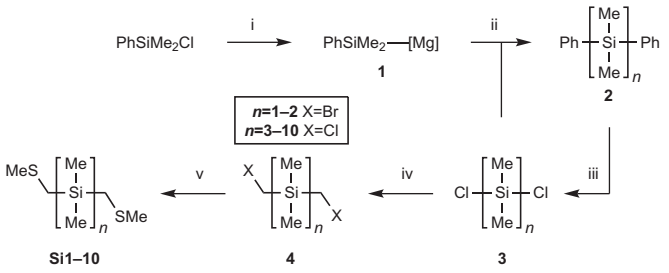

Figure 2 | Iterative synthesis of oligosilanes terminated with methylthiomethyl end groups. More detail on the synthetic methods used here is given in the Supplementary Sections III and IV. i, Li, THF, 0 °C; *i*PrMgCl, 0 °C. ii, **3**, THF, 0 °C; n = 3–10 were synthesized in 60–84% yield. iii, For n = 3 and 4, HCl, $AlCl_3$, toluene, r.t.; for n = 5–10, CF_3SO_3H, dichloromethane, 0 °C; NEt_3·HCl, Et_2O, 0 °C; 64–77% yield. iv, For n = 1 and 2, LiBr, CH_2Br_2, *n*-BuLi, THF, −78 °C; for n = 3–10, CH_2BrCl, *n*-BuLi, THF, −78 °C; 48–93% yield. v, NaSMe, EtOH, 0 °C; 11–86% yield.

from the commercially available mono- and disilanes, respectively. We functionalized α,ω-dichlorooligosilane **3** with electrode linkers (CH_2SMe) in two steps. We installed the halomethyl groups in α,ω-bis(halomethyl)oligosilane **4** by generating the halomethyllithium in the presence of **3**[19,20]. We obtained the final α,ω-bis(methylthiomethyl)oligosilanes **Si1**–**Si10** from nucleophilic substitution of the primary halide with sodium thiomethoxide[21].

STM-BJ conductance measurements. We measured the single-molecule conductance of **Si1**–**Si10** using the STM-BJ technique (see the Supplementary Section V for more details)[22]. The STM-BJ measurement proceeds as follows: point contacts between the Au STM tip and the substrate electrodes are repeatedly broken and formed in a solution of the target molecule (0.05–1.00 mM in 1,2,4-trichlorobenzene) at room temperature and under ambient conditions. After the Au–Au point contact is broken, aurophilic thiomethyl groups[23] on the molecule bridge the electrodes to form an Au–molecule–Au junction. Conductance is measured across the gap as a function of the tip–substrate displacement, and the resulting traces reveal molecule-dependent plateaus that signify junction formations with conductance values below G_0 ($2e^2/h$), the quantum of conductance, where e is charge of an electron and h is Planck's constant[24]. The molecular junction breaks once the tip–substrate electrode gap becomes too wide for the molecule to coordinate to both electrodes. Thousands of molecular junctions are analysed using logarithm-binned one-dimensional (1D) and two-dimensional (2D) histograms. 1D histograms provide a distribution of all measured conductance values from all traces; 2D histograms sum all the conductance values and retain the relative displacement information[25].

The 1D conductance histograms for **Si1**–**Si10** are compiled in Fig. 3a. All the oligosilanes (n = 1–10) gave the same general peak shape: a sharp maximum at higher conductance followed by a broad tail at lower conductance. There is an exponential decrease in conductance as n increases; we quantified this decrease by deriving the length-dependent conductance decay value (β)[26,27]. Figure 3b shows a plot of the conductance maxima from the 1D histograms against each oligomer's effective molecular length (L). L is defined as the distance between the two distal methylenes in each density functional theory (DFT)-optimized structure. We obtain β by fitting a line through these points on a semi-log scale. Figure 3b shows that the conductances of **Si1**–**Si10** fit to a line with $\beta = 0.39 \pm 0.01$ Å^{-1} (more detail regarding the different β values for oligosilanes with thioanisole and methylthiomethyl contacts is given in the Supplementary Section II, Part I). As a comparison, linear alkanes terminated with thiomethyl linkers have a β value of 0.70 ± 0.03 Å^{-1} (ref. 23). This difference arises from the increased σ delocalization that occurs in Si compared with C, as bonding orbitals increase in size and energy down the periodic table[28,29]. As we show below, this additional delocalization in the silanes enables us to observe different conductance values for two distinct sets of rotational isomers in a single molecule.

We defined L in this study as the distance between the distal methylenes in **Si1**–**Si10** to compare the results with our previous study of oligosilanes that have thioanisole linkers, in which L was defined as the distance between the two aryl carbons that terminated the silane chain[26]. By extrapolating our fit to $L = 0$, we found that the contact resistance of the methylthiomethyl linker (0.95 MΩ) was two orders of magnitude smaller than that of our previous thioanisole linker (83 MΩ). The low contact resistance of the methylthiomethyl linkers enabled us to measure the longer oligosilanes in this study and, more importantly, to show that the conductance mechanism in these longer silane chains occurs through non-resonant transport, as evidenced by the clear exponential dependence of conductance with length[30].

Analysis of switching behaviour. For each silane (**Si1** to **Si10**) a large fraction of traces showed an abrupt jump from a lower to a higher value of conductance as the tip–substrate electrode gap widened. Although a similar effect has been observed before in other systems[31–33], it is uncommon; molecular junctions do not typically demonstrate this inverted conductance behaviour. Figure 3c demonstrates this effect in individual traces. 2D histograms allow us to interpret conductance as a function of electrode displacement. We compiled our 2D histograms from traces that exhibited a switch from low to high conductance. Figure 3d depicts such a histogram for **Si4**, in which switching from low to high conductance occurs on elongation in 50% of 6,000 total traces in which we observe a clear molecular conductance plateau (Supplementary Fig. 1 gives the 2D histograms for the other oligosilanes). We defined the point of zero relative displacement as the point along the elongation trajectory at which switching occurs (Fig. 3d). Aligning the traces to the switching event enabled us to sort the histogram into two regimes: the lower-conducting (low G) pre-switch state (where $x < 0$) and the higher-conducting (high G) post-switch state (where $x > 0$). The inset of Fig. 3d shows the 1D histograms that resulted from this separation of the low and high G states (grey and black lines, respectively). The high G peak is sharp and the low G peak is broad. The inset reveals that the sharp peak and broad tail characteristic of each oligosilane arises from the superposition of these two distinct conductance states: in each case a broad low-conductance peak and a sharp high-conductance peak combine to give the asymmetric peak seen in Fig. 3a. The conductances of the low and high G peaks for each oligosilane are plotted against molecular length in Supplementary Fig. 2. Both states decay across the series with the same β value, but in each member of the series the two conductance values differ by about a factor of two.

These molecular switches are robust; we can exercise them in real time. We performed five consecutive compression–elongation cycles in **Si6** in which we compressed and retracted the Au–**Si6**–Au junction near the point of full extension (Fig. 3e,f). In each cycle we elongated the molecular junction fully, held the junction in place for 50 ms, compressed the electrodes by 1.9 Å and then held the junction at this new displacement for another 50 ms (we chose the 1.9 Å distance by which we compressed and elongated these junctions from the 2D histogram shown in Supplementary Fig. 1, which shows the extent of the high G state). Figure 3e shows a compilation of our results over 10,600 traces that started at a conductance that corresponded to the peak shown in the histogram in Fig. 3a. The majority of these traces switched

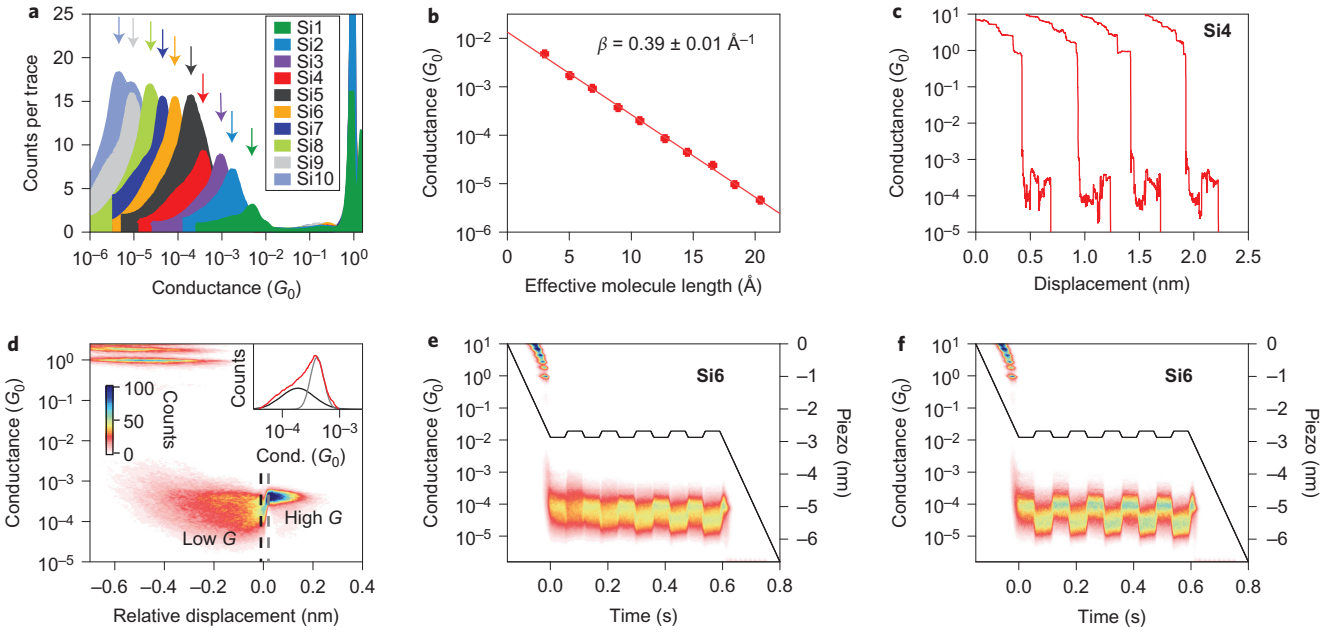

Figure 3 | Conductance analysis of the oligosilane series. a, Logarithm-binned 1D histograms for **Si1**–**Si10**. The arrows denote the peak maxima used for **b**. All the histograms are normalized by the number of traces used to construct the histograms. **b**, Conductance peak values for **Si1**–**Si10** plotted against the effective molecule length give the decay constant β. **c**, Individual traces from the measurement of **Si4** as the electrode displacement increases. Sample traces are offset along the displacement axis for clarity. **d**, 2D conductance–displacement histogram for **Si4** compiled from traces that demonstrate switching. The inset is a compilation of the pre-switching (black line) and post-switching (grey line) regions into 1D histogram plots; the total 1D histogram for **Si4** (red line) is superimposed for comparison. **e**,**f**, 2D histograms of compression–elongation cycles for the Au–**Si6**–Au junction. A modified piezo ramp (black line) is applied to induce switching. Traces are aligned to the beginning of the first hold period. **e**, 2D histogram constructed from all traces for which a molecule remains in the junction during all the hold periods. No other selection was applied. Switching sharpens with each oscillation. **f**, Clean switching from the first to last oscillation occurs in 33% of traces.

between a high and low state, as is clearly visible in the 2D histogram. Further, we observed a 'burn in' effect in which switching between the states became sharper with each additional compression–elongation cycle. This behaviour suggests that the oscillation cycles are training[34] our device by reorganizing the junction into a new environment in which it behaves more effectively as a switch. Clean switching from the first to last elongation–compression cycle occurs in about one-third of traces (Fig. 3f). We performed a single compression–elongation cycle on **Si6** and compared our results with those for 1,8-bis(thiomethyl)octane (**C8**), which has the same –CH_2SMe linker as **Si6** but an aliphatic carbon backbone between the linkers (Supplementary Fig. 3). Although the Au–**Si6**–Au junction demonstrates two-state conductance switching with the conductance increasing on elongation, the Au–**C8**–Au junction maintains a relatively constant conductance over the course of the cycle and shows only a small decrease in conductance on elongation, probably because of a decrease in the through-space conductance component[35–38].

We can begin to understand why switching occurs as the junction elongates by comparing the 2D histogram characteristics of the low and high G states across the oligosilane series (Supplementary Fig. 1). First, conductance changes by a factor of two for all oligosilanes regardless of the length of the Si chain. Second, the length of the conductance-plateau characteristic of the low G state increases from **Si1** to **Si10** (1 Å for **Si1** to 10 Å for **Si10**), whereas that of the high G state stays relatively constant (1.5–2.0 Å). The consistency in the switching ratio and high G length across the entire oligosilane series suggests that the high G state arises from a molecular feature that is common to all oligomers and invariant among them. We therefore do not believe that the switching we observed here arose from sudden rotations of the internal Si–Si–Si–Si dihedral geometries (see the Supplementary Section II, Part II for more analysis)[39–41]. Given these details and the stereoelectronics of bonding around sulfur[42], we hypothesize that the stereoelectronic effects of the two terminal dihedral angles (H_3C–S–CH_2–$SiMe_2$–) that terminate each oligosilane are fundamentally responsible for the switching we observed here. These dihedral angles should be particularly susceptible to changes in the tip–substrate distance because they involve gold atoms from the electrodes exerting torque on the molecule via the sulfur lone pair.

DFT analysis. We examined the effect of electrode displacement on molecular geometry in a DFT model system (see the Supplementary Section VI for details)[43]. In this model we attached single Au atoms to both sulfur atoms in **Si4** to simulate the bonding to Au electrodes and varied the Au–to–Au distance. In the STM-BJ experiment the two Au electrodes perform two distinct, albeit closely related, functions: (1) they provide the electrical environment through which the current passes, and (2) they dictate the geometry of the included molecule. Our computational model describes both features. We first performed geometry optimizations to determine how the lowest energy conformation of the molecule changes on increasing the Au–Au distance. To model the influence that the Au electrodes have on the geometry of the molecule, we considered the [Au–**Si4**–Au]$^{2+}$ model system (removing two electrons from the complex) to increase the Au–S bond strength and mimic binding to a slightly positive undercoordinated Au atom on an Au electrode[23].

Model calculations on the free trimethyl(methylsulfanylmethyl)-silane (Me–S–CH_2–$SiMe_3$) molecule demonstrated two isoenergetic local minima at 90° and 270° (*ortho*) and a global minimum at 180° (*anti*), as expected from simple stereoelectronic considerations (Supplementary Fig. 4). We therefore set both dihedral angles to *anti* in our starting geometry, optimized the [Au–**Si4**–Au]$^{2+}$

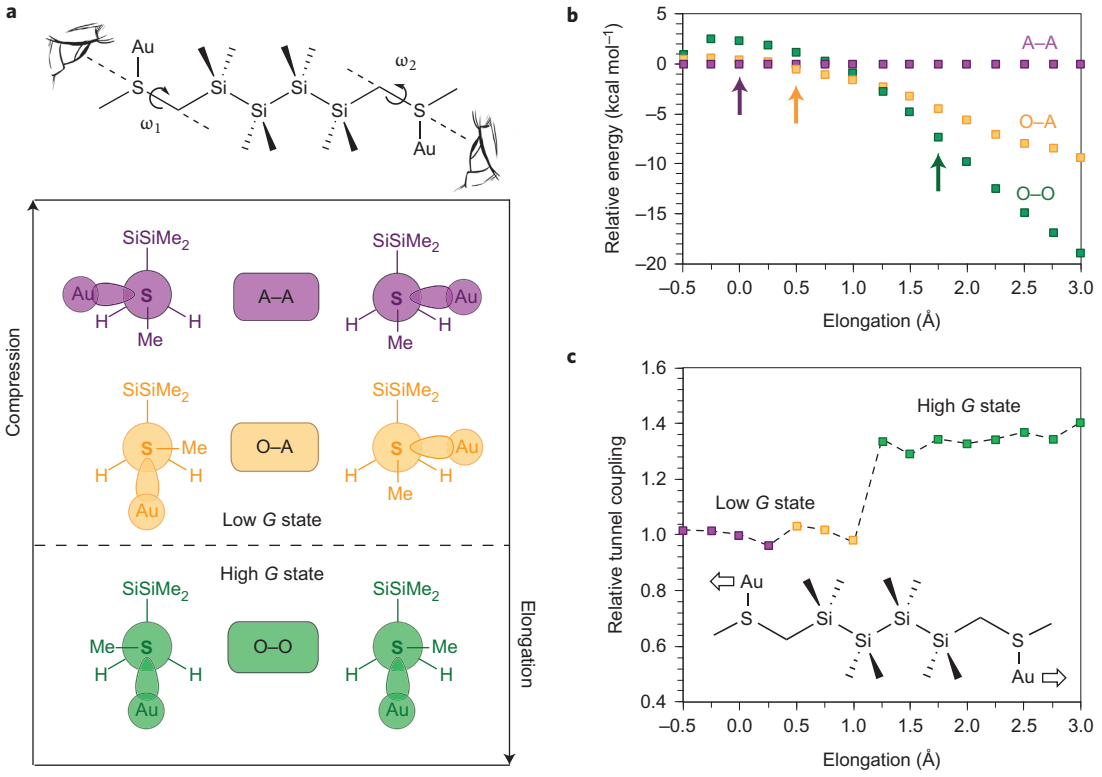

Figure 4 | DFT calculations describe the mechanism for switching as the oligosilanes are elongated in the junction. a, Newman projections for the A–A (purple), O–A (yellow) and O–O (green) dihedral configurations from the perspective of the sulfur–methylene σ bond in the Au–**Si4**–Au system. Junction elongation strains the molecule into the higher conducting O–O conformer. **b**, The relative energies of the A–A, O–A and O–O conformers in the $[Au\text{–}Si4\text{–}Au]^{2+}$ model system (B3LYP/LACVP**) are obtained by subtracting the total energy of the A–A conformer at each particular Au–Au distance. The coloured arrows denote the specific Au–Au distance at which each configuration experiences its lowest total energy. **c**, Tunnel coupling as a function of the Au–Au distance plotted relative to tunnel coupling at the elongation = 0 point for the Au–**Si4**–Au model system (B3LYP/LACVP**). Tunnel-coupling calculations were performed on the lowest-energy geometries optimized without dihedral constraint.

complex without constraint and defined the resulting Au–Au distance as the elongation = 0 point (Fig. 4b,c). We then performed a series of calculations to understand the response of the **Si4** bridge to changes in the Au–Au gap. To obtain the lowest energy structure at each Au–Au distance, we varied the (fixed) Au–Au distance in 0.25 Å increments while allowing the rest of the molecule to optimize its geometry without additional constraints.

These geometry optimizations confirm that the terminal dihedral orientation depends strongly on the distance between the Au atoms (that is, the size of the interelectrode gap). Just as in the free Me–S–CH_2–$SiMe_3$ molecule, there are two distinct *anti* and *ortho* Me–S–CH_2–$SiMe_2$– dihedral geometries in our Au–**Si4**–Au model. The *anti* (A) geometry places the Me–S bond antiperiplanar (Au–S bond is perpendicular) to the CH_2–$SiMe_2$ bond; the *ortho* (O) geometry places the Me–S bond perpendicular (Au–S bond is antiperiplanar) to the CH_2–$SiMe_2$ bond (Fig. 4a). The results of our geometry optimizations suggest that there are two competing sources of strain: steric strain from the S–CH_2 σ-bond stereochemistry and mechanical strain from electrode separation. Steric strain favours the *anti* geometry because it minimizes steric repulsion between the bulky S-methyl and $SiMe_2$ groups. Mechanical strain pulls the S–Au bond into an antiperiplanar position to adopt the longest possible molecular geometry, and thereby forces the S-methyl group into an *ortho* relationship with the $SiMe_2$ group. As the mechanical strain starts to eclipse the steric strain, the two terminal Me–S–CH_2–$SiMe_2$ dihedral angles in the lowest-energy Au–**Si4**–Au geometries change, as shown in Fig. 4a, from A–A (purple) to O–A (yellow) to O–O (green).

The competing effect of steric versus mechanical strain on the molecular geometry is evident in Fig. 4b. We fixed the terminal dihedrals to A–A, O–A and O–O to demonstrate how the relative energies of these three configurations change as a function of Au–Au distance. At short distances the steric strain has a stronger influence on molecular geometry: the A–A configuration is the lowest in energy and the energy difference between each conformational state is relatively small. As the distance between the Au atoms increases and more mechanical strain is imposed on the molecule, the O–O configuration becomes the most energetically stable state and the energy differences between the three conformers become relatively large.

To determine the trends in conductance for the lowest-energy structures that occur at each Au–Au distance, we calculated the energy splitting between the frontier molecular orbitals of the neutral Au–molecule–Au complex. The frontier orbitals are predominantly of Au 6*s* and S lone-pair antibonding character and are tunnel-coupled through the molecular backbone, which results in a symmetric and antisymmetric pair with a splitting of $2t$, where t is defined as the tunnel coupling parameter[27]. The square of the tunnel coupling has been shown to be proportional to molecular conductance for many different systems[27,44–50]. We plot in Fig. 4c the square of the tunnel coupling ($4t^2$) for the Au–**Si4**–Au geometries relative to the elongation = 0 point. Conductance reflects the strength of coupling between the two gold electrodes through the molecule. We have shown previously that the Si–Si σ-bond framework provides the orbital through which the electron tunnels in an oligosilane[26]. Considering these two factors, one would predict a lower conductivity for the A–A and O–A configurations because the

anti dihedral describes a S–Au bond that is perpendicular to the plane of the Si–Si bonds and therefore poorly coupled to the rest of the molecule. Conversely, one would predict higher conductivity for the O–O configuration because both S–Au bonds are aligned with the neighbouring C–Si bonds, and therefore the entire set of Si–Si bonds in the molecule.

This intuition rationalizes why the tunnel coupling remains constant as the minimum geometry transitions from A–A to O–A, but increases significantly as the molecule transitions from O–A to O–O (Fig. 4c). In the O–O state, both Au atoms are finally aligned for coupling through the strong σ conjugation in the silane backbone. This interpretation implies that, even though there are three conformational states (A–A, O–A and O–O), we only observe a two-state conductance system because the A–A and O–A conformers have a similar tunnel coupling and are therefore indistinguishable in the junction.

We applied the same DFT treatment to 1,6-bis(thiomethyl) hexane (**C6**) and found that the same conformational shift from A–A to O–A to O–O states occurred as we increased the Au–Au distance; however, the tunnel coupling remained constant because the poorly conjugated C–C σ bonds did not improve the coupling between the Au atoms in the O–O dihedral configuration (Supplementary Fig. 5). The experimental implication is that, even though this three-state conformational system exists in alkanes, we only observe a one-state electronic system because all three dihedral conformers are indistinguishable in conductance. The strong σ conjugation in the oligosilane backbone electronically couples the linker dihedrals that terminate each end of the molecule—we can therefore resolve the conductances of two different sets of rotational isomers that arise from the stereoelectronics of the sulfur–methylene σ bond and switch between them by stretching and compressing our molecular junction.

Conclusions

The canons of σ stereoelectronics were developed to understand the relationship between conformation and electronics in aliphatic systems. However, the weak conjugation in C–C σ bonds diminishes the utility of stereoelectronics in controlling charge transport through aliphatic wires. In this study, we demonstrate that the strong conjugation in Si–Si σ bonds enables us to observe and exploit stereoelectronic effects in single-molecule junctions. The oligosilane switches developed here are the first in a new class of stereoelectronic device components; these switches function from the stereoelectronic properties of the sulfur–methylene σ bond. We can transpose the σ-stereoelectronic models originally devised for alkanes to silanes because they share a similar tetrahedral bonding geometry. We therefore envision that many more silicon-based electronic components inspired from the expansive σ-stereoelectronics literature will soon be realized.

Methods

All DFT computations in this manuscript were carried out with Jaguar (version 8.3, Schrodinger). All synthetic methods, characterization, STM-BJ experiments and analysis details, and DFT computational details are given in the Supplementary Information.

Received 15 October 2014; accepted 9 January 2015; published online 16 February 2015

References

1. Reed, M. A. & Tour, J. M. Computing with molecules. *Sci. Am.* **282,** 86–93 (2000).
2. Song, H., Reed, M. A. & Lee, T. Single molecule electronic devices. *Adv. Mater.* **23,** 1583–1608 (2011).
3. Turro, N. J. *Modern Molecular Photochemistry* (University Science Books, 1991).
4. Butenhoff, T. J. & Moore, C. B. Hydrogen atom tunneling in the thermal tautomerism of porphine imbedded in a *n*-hexane matrix. *J. Am. Chem. Soc.* **110,** 8336–8341 (1988).
5. Phelan, N. F. & Orchin, M. Cross conjugation. *J. Chem. Educ.* **45,** 633–637 (1968).
6. Van der Molen, S. J. *et al.* Light-controlled conductance switching of ordered metal–molecule–metal devices. *Nano Lett.* **9,** 76–80 (2009).
7. Auwärter, W. *et al.* A surface-anchored molecular four-level conductance switch based on single proton transfer. *Nature Nanotechnol.* **7,** 41–46 (2012).
8. Darwish, N. *et al.* Observation of electrochemically controlled quantum interference in a single anthraquinone-based norbornylogous bridge molecule. *Angew. Chem. Int. Ed.* **51,** 3203–3206 (2012).
9. Eliel, E. L. & Wilen, S. H. *Stereochemistry of Organic Compounds* (Wiley, 1994).
10. Choi, B-Y. *et al.* Conformational molecular switch of the azobenzene molecule: a scanning tunneling microscopy study. *Phys. Rev. Lett.* **96,** 156106 (2006).
11. Donhauser, Z. J. *et al.* Conductance switching in single molecules through conformational changes. *Science* **292,** 2303–2307 (2001).
12. Moore, A. M. *et al.* Molecular engineering and measurements to test hypothesized mechanisms in single molecule conductance switching. *J. Am. Chem. Soc.* **128,** 1959–1967 (2006).
13. Blum, A. S. *et al.* Molecularly inherent voltage-controlled conductance switching. *Nature Mater.* **4,** 167–172 (2005).
14. Rahimi, M. & Troisi, A. Probing local electric field and conformational switching in single-molecule break junctions. *Phys. Rev. B* **79,** 113413 (2009).
15. Moresco, F. *et al.* Conformational changes of single molecules induced by scanning tunneling microscopy manipulation: a route to molecular switching. *Phys. Rev. Lett.* **86,** 672–675 (2001).
16. Franco, I., Solomon, G. C., Schatz, G. C. & Ratner, M. A. Tunneling currents that increase with molecular elongation. *J. Am. Chem. Soc.* **133,** 15714–15720 (2011).
17. Shibano, Y. *et al.* Conformation effect of oligosilane linker on photoinduced electron transfer of tetrasilane-linked zinc porphyrin–[60]fullerene dyads. *J. Organomet. Chem.* **692,** 356–367 (2007).
18. Ruehl, K. E. & Matyjaszewski, K. Dearylation of α,ω-diphenylpermethylated oligosilanes with triflic acid. *J. Organomet. Chem.* **410,** 1–12 (1991).
19. Kobayashi, T. & Pannell, K. H. A general, high-yield reaction for the formation of (chloromethyl)oligosilanes. *Organometallics* **9,** 2201–2203 (1990).
20. Kobayashi, T. & Pannell, K. H. Synthesis of (chloromethyl)silanes by the low-temperature reaction of chlorosilanes and *in situ* generated (chloromethyl) lithium in tetrahydrofuran. *Organometallics* **10,** 1960–1964 (1991).
21. Anklam, E. Synthese von α-Halogen-ω-alkylthio-alkanen und α,ω-Bisalkylthio-alkanen. *Synthesis* **1987,** 841–843 (1987).
22. Xu, B. & Tao, N. J. Measurement of single-molecule resistance by repeated formation of molecular junctions. *Science* **301,** 1221–1223 (2003).
23. Park, Y. S. *et al.* Contact chemistry and single-molecule conductance: a comparison of phosphines, methyl sulfides, and amines. *J. Am. Chem. Soc.* **129,** 15768–15769 (2007).
24. Agraït, N., Rodrigo, J. & Vieira, S. Conductance steps and quantization in atomic-size contacts. *Phys. Rev. B* **47,** 12345–12348 (1993).
25. Gonzalez, M. T. *et al.* Electrical conductance of molecular junctions by a robust statistical analysis. *Nano Lett.* **6,** 2238–2242 (2006).
26. Klausen, R. S., Widawsky, J. R., Steigerwald, M. L., Venkataraman, L. & Nuckolls, C. Conductive molecular silicon. *J. Am. Chem. Soc.* **134,** 4541–4544 (2012).
27. Hybertsen, M. S. *et al.* Amine-linked single-molecule circuits: systematic trends across molecular families. *J. Phys. Condens. Matter* **20,** 374115 (2008).
28. Sandorfy, C. LCAO MO calculations on saturated hydrocarbons and their substituted derivatives. *Can. J. Chem.* **33,** 1337–1351 (1955).
29. Schepers, T. & Michl, J. Optimized ladder C and ladder H models for sigma conjugation: chain segmentation in polysilanes. *J. Phys. Org. Chem.* **15,** 490–498 (2002).
30. Salomon, A. *et al.* Comparison of electronic transport measurements on organic molecules. *Adv. Mater.* **15,** 1881–1890 (2003).
31. Temirov, R., Lassise, A., Anders, F. B. & Tautz, F. S. Kondo effect by controlled cleavage of a single-molecule contact. *Nanotechnology* **19,** 065401 (2008).
32. Bruot, C., Hihath, J. & Tao, N. Mechanically controlled molecular orbital alignment in single molecule junctions. *Nature Nanotechnol.* **7,** 35–40 (2012).
33. González, M. T. *et al.* Stability of single- and few-molecule junctions of conjugated diamines. *J. Am. Chem. Soc.* **135,** 5420–5426 (2013).
34. Trouwborst, M., Huisman, E., Bakker, F., van der Molen, S. & van Wees, B. Single atom adhesion in optimized gold nanojunctions. *Phys. Rev. Lett.* **100,** 175502 (2008).
35. Chang, S., He, J., Zhang, P., Gyarfas, B. & Lindsay, S. Gap distance and interactions in a molecular tunnel junction. *J. Am. Chem. Soc.* **133,** 14267–14269 (2011).
36. Lin, J. & Beratan, D. N. Tunneling while pulling: the dependence of tunneling current on end-to-end distance in a flexible molecule. *J. Phys. Chem. A* **108,** 5655–5661 (2004).
37. Lafferentz, L. *et al.* Conductance of a single conjugated polymer as a continuous function of its length. *Science* **323,** 1193–1197 (2009).
38. Fan, F-R. F. *et al.* Charge transport through self-assembled monolayers of compounds of interest in molecular electronics. *J. Am. Chem. Soc.* **124,** 5550–5560 (2002).

39. Piqueras, M. C., Crespo, R. & Michl, J. The transoid, ortho, and gauche conformers of decamethyl-*n*-tetrasilane, *n*-Si_4Me_{10}: electronic transitions in the multistate complete active space second-order perturbation theory description. *J. Phys. Chem. A* **107,** 4661–4668 (2003).
40. George, C. B., Ratner, M. A. & Lambert, J. B. Strong conductance variation in conformationally constrained oligosilane tunnel junctions. *J. Phys. Chem. A* **113,** 3876–3880 (2009).
41. Michl, J. & West, R. Conformations of linear chains. Systematics and suggestions for nomenclature. *Acc. Chem. Res.* **33,** 821–823 (2000).
42. Goddard, W. A. & Harding, L. B. The description of chemical bonding from *ab initio* calculations. *Annu. Rev. Phys. Chem.* **29,** 363–396 (1978).
43. Jaguar, version 8.3 (Schrodinger, Inc., New York, 2014).
44. Parameswaran, R. *et al.* Reliable formation of single molecule junctions with air-stable diphenylphosphine linkers. *J. Phys. Chem. Lett.* **1,** 2114–2119 (2010).
45. McConnell, H. M. Intramolecular charge transfer in aromatic free radicals. *J. Chem. Phys.* **35,** 508–515 (1961).
46. Woitellier, S., Launay, J. P. & Joachim, C. The possibility of molecular switching: theoretical study of $[(NH_3)_5Ru\text{-}4,4'\text{-}bipy\text{-}Ru(NH_3)_5]^{5+}$. *Chem. Phys.* **131,** 481–488 (1989).
47. Venkataraman, L. *et al.* Electronics and chemistry: varying single-molecule junction conductance using chemical substituents. *Nano Lett.* **7,** 502–506 (2007).
48. Venkataraman, L., Klare, J. E., Nuckolls, C., Hybertsen, M. S. & Steigerwald, M. L. Dependence of single-molecule junction conductance on molecular conformation. *Nature* **442,** 904–907 (2006).
49. Venkataraman, L. *et al.* Single-molecule circuits with well-defined molecular conductance. *Nano Lett.* **6,** 458–462 (2006).
50. Park, Y. S. *et al.* Frustrated rotations in single-molecule junctions. *J. Am. Chem. Soc.* **131,** 10820–10821 (2009).

Acknowledgements

We thank the National Science Foundation (NSF) for the primary support of these studies under Grant No. CHE-1404922. T.A.S. is supported by the NSF Graduate Research Fellowship under Grant No. 11-44155. H.L. is supported by the Semiconductor Research Corporation and New York Center for Advanced Interconnect Science and Technology program. L.V. thanks the Packard Foundation for support. We thank R. S. Klausen, P. Mortimer and Y. Itagaki for mass spectrometry assistance and O. Adak, E. J. Dell and J. L. Leighton for insightful discussions.

Author contributions

T.A.S. synthesized all the molecules. H.L. carried out all the STM-BJ measurements. T.A.S. and M.L.S. carried out all the computations. All the authors conceived the idea, designed the experiments, analysed the data and co-wrote the manuscript.

Additional information

Supplementary information and chemical compound information are available in the online version of the paper. Reprints and permissions information is available online at www.nature.com/reprints. Correspondence and requests for materials should be addressed to M.L.S., L.V. and C.N.

Competing financial interests

The authors declare no competing financial interests.